Astronomy & Astrophysics manuscript no. LMC
January 9, 2017
©ESO 2017

arXiv:1701.01604v1 [astro-ph.GA] 6 Jan 2017

Kinetic temperature of massive star forming molecular clumps measured with formaldehyde. II. The Large Magellanic Cloud

X. D. Tang[1, 2, 3], C. Henkel[1, 4], C. -H. R. Chen[1], K. M. Menten[1], R. Indebetouw[5, 6], X. W. Zheng[7], J. Esimbek[2, 3], J. J. Zhou[2, 3], Y. Yuan[2, 3], D. L. Li[2, 3], and Y. X. He[2, 3]

[1] Max-Planck-Institut für Radioastronomie, Auf dem Hügel 69, 53121 Bonn, Germany
e-mail: xdtang@mpifr-bonn.mpg.de
[2] Xinjiang Astronomical Observatory, Chinese Academy of Sciences, 830011 Urumqi, China
[3] Key Laboratory of Radio Astronomy, Chinese Academy of Sciences, 830011 Urumqi, China
[4] Astronomy Department, King Abdulaziz University, PO Box 80203, 21589 Jeddah, Saudi Arabia
[5] National Radio Astronomy Observatory, 520 Edgemont Rd, Charlottesville, VA 22903, USA
[6] University of Virginia, Charlottesville, VA 22903, USA
[7] Department of Astronomy, Nanjing University, 210093 Nanjing, China

January 9, 2017

ABSTRACT

Context. The kinetic temperature of molecular clouds is a fundamental physical parameter affecting star formation and the initial mass function. The Large Magellanic Cloud (LMC), the closest star forming galaxy with low metallicity, provides an ideal laboratory to study star formation in such an environment.

Aims. The classical dense molecular gas thermometer NH_3 is rarely available in a low metallicity environment because of photoionization and a lack of nitrogen atoms. Our goal is to directly measure the gas kinetic temperature with formaldehyde toward six star-forming regions in the LMC.

Methods. Three rotational transitions ($J_{K_AK_C}$ = 3_{03}-2_{02}, 3_{22}-2_{21}, and 3_{21}-2_{20}) of para-H_2CO near 218 GHz were observed with the Atacama Pathfinder EXperiment (APEX) 12 m telescope toward six star forming regions in the LMC. Those data are complemented by $C^{18}O$ 2-1 spectra.

Results. Using non-LTE modeling with RADEX, we derive the gas kinetic temperature and spatial density, using as constraints the measured para-H_2CO 3_{21}-2_{20}/3_{03}-2_{02} and para-H_2CO 3_{03}-2_{02}/$C^{18}O$ 2-1 ratios. Excluding the quiescent cloud N159S, where only one para-H_2CO line could be detected, the gas kinetic temperatures derived from the preferred para-H_2CO 3_{21}-2_{20}/3_{03}-2_{02} line ratios range from 35 to 63 K with an average of 47 ± 5 K (errors are unweighted standard deviations of the mean). Spatial densities of the gas derived from the para-H_2CO 3_{03}-2_{02}/$C^{18}O$ 2-1 line ratios yield 0.4 – 2.9 × 10^5 cm^{-3} with an average of 1.5 ± 0.4 × 10^5 cm^{-3}. Temperatures derived from the para-H_2CO line ratio are similar to those obtained with the same method from Galactic star forming regions and agree with results derived from CO in the dense regions ($n(H_2) > 10^3$ cm^{-3}) of the LMC. A comparison of kinetic temperatures derived from para-H_2CO with those from the dust also shows good agreement. This suggests that the dust and para-H_2CO are well mixed in the studied star forming regions. A comparison of kinetic temperatures derived from para-H_2CO 3_{21}-2_{20}/3_{03}-2_{02} and NH_3(2,2)/(1,1) shows, however, a drastic difference. In the star forming region N159W, the gas temperature derived from the NH_3(2,2)/(1,1) line ratio is ∼16 K (Ott et al. 2010), which is only half the temperature derived from para-H_2CO and the dust. Furthermore, ammonia shows a very low abundance in a 30″ beam. Apparently, ammonia only survives in the most shielded pockets of dense gas not yet irradiated by UV photons, while formaldehyde, less affected by photodissociation, is more widespread and is also sampling regions more exposed to the radiation of young massive stars. A correlation between the gas kinetic temperatures derived from para-H_2CO and infrared luminosity, represented by the 250 μm flux, suggests that the kinetic temperatures traced by para-H_2CO are correlated with the ongoing massive star formation in the LMC.

Key words. Galaxies: star formation – Galaxies: Magellanic Clouds – Galaxies: ISM – Galaxies: irregular – ISM: molecules – radio lines: ISM

1. Introduction

The Large Magellanic Cloud (LMC), at a distance of ∼50 kpc (Pietrzyński et al. 2013), is the nearest low metallicity (Rolleston 2002) star-forming galaxy to the Milky Way. The relatively face-on view offered by the LMC provides an ideal perspective to study star formation, particularly massive star formation associated with its numerous stellar clusters. In the LMC, the FUV field is stronger than in the Milky Way (Westerlund 1990). It is thus well suited to study the properties of the interstellar medium, the evolution of molecular clouds, and star for-

mation in an active low metallicity galaxy, also providing a link to galaxies at high redshift.

The physical properties of the molecular gas in the LMC, in particular the kinetic temperature, are not well constrained. The easily thermalized and optically thick rotational CO transitions are good temperature tracers of the cold and dense gas in local clouds. Generally, however, they often suffer from a lack of information on the beam filling factor in extragalactic clouds. Multi-level observations of suitable molecules deliver the most reliable temperature determinations. The metastable lines of ammonia (NH_3) are frequently used as the standard molecular cloud thermometer in molecular clouds within our Galaxy and also in external galaxies (Ho & Townes 1983; Walmsley & Ungerechts 1983; Danby et al. 1988; Henkel et al. 2000, 2008; Weiß et al. 2001; Mauersberger et al. 2003; Ao et al. 2011; Lebrón et al. 2011; Ott et al. 2011; Wienen et al. 2012; Mangum et al. 2013a). However, the ammonia abundance can vary strongly in different molecular environments (e.g., 10^{-5} in dense, molecular "hot cores" around newly formed massive stars, Mauersberger et al. 1987; 10^{-8} in dark clouds, Benson & Myers 1983; Chira et al. 2013; 10^{-10} in a massive star forming cloud of the LMC, Ott et al. 2010) and is extremely affected by a high UV flux. Thus, in a low metallicity environment with high UV flux and a lack of shielding dust grains, ammonia is of limited use as a reliable probe to trace the gas kinetic temperature. To make this problem even more severe, the LMC is also a galaxy with particulary low nitrogen abundance (∼10% solar, Wang et al. 2009; Ott et al. 2010).

Formaldehyde (H_2CO) is a ubiquitous molecule in the Galactic interstellar medium (ISM) of our and external galaxies (Downes et al. 1980; Cohen & Few 1981; Bieging et al. 1982; Cohen et al. 1983; Baan et al. 1986, 1990, 1993; Henkel et al. 1991; Zylka et al. 1992; Hüttemeister et al. 1997; Heikkilä et al. 1999; Wang et al. 2004, 2009; Mangum et al. 2008; Zhang et al. 2012; Mangum et al. 2013b; Ao et al. 2013; Tang et al. 2013; Ginsburg et al. 2015, 2016; Guo et al. 2016). H_2CO is thought to be formed on the surface of dust grains by successive hydrogenation of CO (Watanabe & Kouchi 2002; Woon 2002; Hidaka et al. 2004): CO → HCO → H_2CO. Variations of the fractional abundance of H_2CO do not exceed one order of magnitude. For example, the fractional abundance of H_2CO is similar across various sub regions of the well-studied Orion-KL nebula, i.e., the "hot core" and the "compact ridge" (Mangum et al. 1990, 1993; Caselli et al. 1993; Johnstone et al. 2003).

Para-H_2CO has a rich variety of millimeter and submillimeter transitions. Line ratios of para-H_2CO involving different K_a ladders are good tracers of the kinetic temperature, such as para-H_2CO J_{KaKc} = 3_{22}-2_{21}/3_{03}-2_{02}, 4_{23}-3_{22}/4_{04}-3_{03}, and 5_{23}-4_{22}/5_{05}-4_{04}, since the relative populations of the K_a ladders of para-H_2CO are predominantly governed by collisions (Mangum & Wootten 1993; Mühle et al. 2007). Among these para-H_2CO lines, the above three transitions with rest frequencies of 218.222, 218.475, and 218.760 GHz, respectively, are particularly useful for use a thermometer, because they are strong enough for extragalactic observations and because they can be measured simultaneously within a bandwidth of 1 GHz. Temperature determined from these ratios are free from uncertainties related to pointing accuracy, calibration or different beam sizes. Since the line emission is optically thin and the levels are located up to 68 K above the ground state, the line ratios are sensitive to gas kinetic temperatures up to 50 K with relatively small uncertainties (Mangum & Wootten 1993; Ao et al. 2013). Para-H_2CO 3–2 line ratios have been used to measure the molecular gas kinetic temperatures in our Galactic center (Qin et al. 2008; Ao et al. 2013; Johnston et al. 2014; Ginsburg et al. 2016; Immer et al. 2016), star formation regions (Mangum & Wootten 1993; Mitchell et al. 2001; Watanabe & Mitchell 2008; Tang et al. 2016), as well as in external galaxies (e.g., Mühle et al. 2007).

Table 1. Source coordinates, integration times, and epochs.

Sources	RA(J2000) h m s	DEC(J2000) ° ′ ″	Int. Time min	Obs. Date
N159W	05:39:35.2	-69:45:37.0	229	July-2008
N113	05:13:17.2	-69:22:23.0	91	September-2008
N44BC	05:22:02.8	-67:57:45.8	68	May-2014
30 Dor	05:38:49.3	-69:04:44.0	64	May-2014
N159S	05:40:02.8	-69:50:32.7	166	May-July-2014
N159E	05:40:04.4	-69:44:34.0	80	July-2014

Multitransition observations of molecular clouds in the LMC (Johansson et al. 1998; Heikkilä et al. 1999; Israel et al. 2003; Kim et al. 2004; Bolatto et al. 2005; Pineda et al. 2008; Mizuno et al. 2010; Minamidani et al. 2008, 2011; Fujii et al. 2014; Paron et al. 2016) suggest that the molecular gas traced by CO may be warmer and/or denser than in our Galaxy. NH_3(1,1) and (2,2) lines have been surveyed toward seven star-forming regions in the LMC by Ott et al. (2010) using the Australia Telescope Compact Array (ATCA). Emission is only detected in the massive star-forming region N159W. This represents so far the only detection of NH_3 in the Magellanic Clouds. The gas kinetic temperature derived from NH_3 (2,2)/(1,1) is cold (∼16 K), which is two times lower than the derived dust temperature 30 – 40 K (Heikkilä et al. 1999; Bolatto et al. 2000; Gordon et al. 2014). Ott et al. (2010) also found a low fractional NH_3 abundance of $\sim 4 \times 10^{-10}$, which is lower by 1.5 – 5 orders of magnitude than those observed in Galactic star-forming regions. Previous observations of formaldehyde have been made in the LMC (e.g., Whiteoak & Gardner 1976; Johansson et al. 1994; Heikkilä et al. 1999; Wang et al. 2009) and H_2CO has been detected in many dense clumps. These observations show that the fractional abundance of para-H_2CO ranges from 1 to 6×10^{-10}, which agrees with the values found in our Galactic molecular clouds (e.g., Güsten & Henkel 1983; Zylka et al. 1992; Johnstone et al. 2003; Ao et al. 2013; Tang et al. 2016).

For this paper, we have carried out deep observations of the six star forming regions 30 Dor, N44BC, N113, N159E, N159S, and N159W in the LMC. Targeting three transitions of para-H_2CO ($J_{K_AK_C}$ = 3_{03}-2_{02}, 3_{22}-2_{21}, and 3_{21}-2_{20}) as well as $C^{18}O$ 2-1 we simultaneously determine kinetic temperatures and spatial densities at high precision. In Sections 2 and 3, we introduce our observations of the para-H_2CO triplet and the data reduction, and describe the main results. These are then discussed in Section 4. Our main conclusions are summarized in Section 5.

2. Observations and data reduction

Our observations were carried out in 2008 and 2014 (summarized in Table 1) with the Atacama Pathfinder EXperiment (APEX) 12 m telescope located on Chajnantor (Chile) using the APEX-1 (SHeFI) receiver. The beam size is ∼30″ (∼7 pc at 50 kpc distance) at 218 GHz. The main beam efficiency and the forward efficiency were 0.75 and 0.97, respectively. N113 and N159W were observed in 2008 with an old Fast Fourier Transform Spectrometer (FFTS), which consists of two units with a bandwidth of 1 GHz each and a velocity resolution of 0.1675

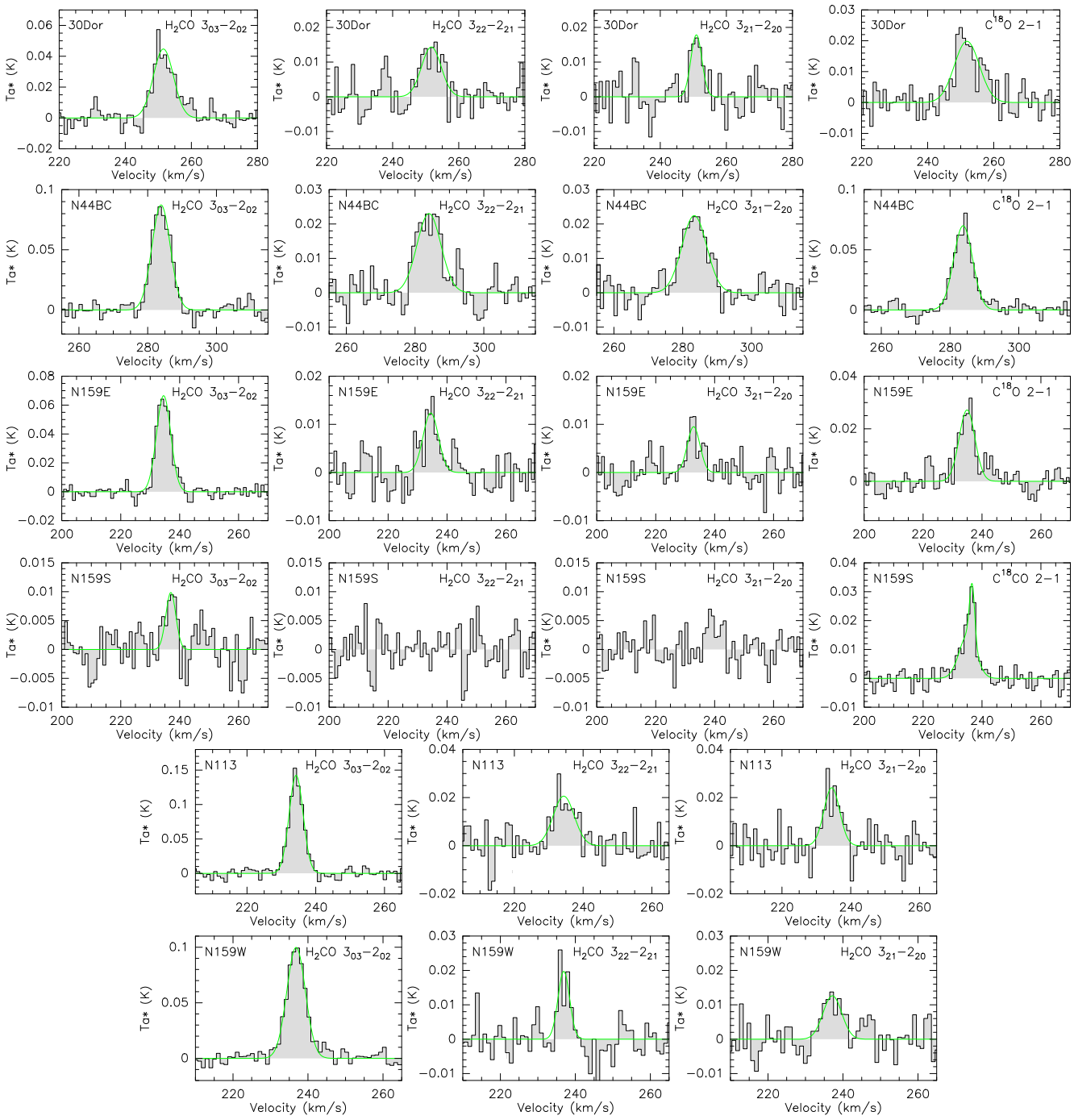

Fig. 1. Para-H_2CO (3_{03}-2_{02}, 3_{22}-2_{21}, and 3_{21}-2_{20}) and $C^{18}O$ (2-1) spectra.

km s^{-1}. The frequency is centered at 218.480 GHz. Our data includes all three of the 218 GHz para-H_2CO lines. 30 Dor, N159E, N159S, and N44BC were observed in 2014. Here we used the new eXtended bandwidth Fast Fourier Transform Spectrometer (XFFTS) backend with two spectral windows of 2.5 GHz bandwidth and a velocity resolution of 0.1047 km s^{-1}. The central frequency is set at 218.550 GHz. These data do not only include the three para-H_2CO lines but also the 219.560 GHz $C^{18}O$ (2-1) transition.

Toward each of the six star forming regions in the LMC Wong et al. (2011) took a single pointing, high sensitivity (∼5 mK rms, T_{mb} scale, beam size ∼30″) spectrum centered on its CO emission peak which will be used to estimate $N(H_2)$ in Section 4.1. Ancillary $C^{18}O$ 2-1 data have been published by Heikkilä et al. (1998) and Wang et al. (2009). In addition, ammonia (NH_3) data from the LMC (Ott et al. 2010) and Herschel infrared data will also play an important role.

Data reduction for spectral lines was performed using CLASS from the GILDAS package[1]. To enhance signal to noise ratios (S/N) in individual channels, we smoothed contiguous channels to a velocity resolution of ∼1.0 km s^{-1}. Sources observed are listed in Table 1.

[1] http://www.iram.fr/IRAMFR/GILDAS

Table 2. Para-H_2CO and $C^{18}O$ spectral parameters[a].

Sources	Molecule	Transition	$\int T_{mb} dv$	V_{lsr}	FWHM[b]	T_{mb}	rms
			K km s^{-1}	km s^{-1}	km s^{-1}	K	mK
30 Dor	H_2CO	$3_{03}-2_{02}$	0.401 (0.026)	250.92 (0.21)	6.12 (0.47)	0.061	6.8
	H_2CO	$3_{22}-2_{21}$	0.114 (0.023)	251.61 (0.70)	6.48 (1.19)	0.017	6.5
	H_2CO	$3_{21}-2_{20}$	0.109 (0.021)	251.01 (0.41)	4.29 (1.00)	0.023	6.4
	$C^{18}O$	2 – 1	0.190 (0.026)	251.25 (0.48)	7.09 (1.34)	0.025	5.6
N113	H_2CO	$3_{03}-2_{02}$	0.930 (0.029)	234.25 (0.07)	4.86 (0.17)	0.181	7.0
	H_2CO	$3_{22}-2_{21}$	0.217 (0.035)	234.40 (0.58)	7.05 (1.20)	0.029	6.9
	H_2CO	$3_{21}-2_{20}$	0.213 (0.025)	234.36 (0.33)	5.69 (0.68)	0.035	7.3
N44BC	H_2CO	$3_{03}-2_{02}$	0.775 (0.026)	283.86 (0.11)	6.37 (0.23)	0.114	6.5
	H_2CO	$3_{22}-2_{21}$	0.155 (0.019)	283.97 (0.45)	6.98(0.88)	0.021	5.2
	H_2CO	$3_{21}-2_{20}$	0.152 (0.021)	283.45 (0.47)	6.50 (0.90)	0.022	5.1
	$C^{18}O$	2 – 1	0.558 (0.022)	283.78 (0.12)	6.08 (0.28)	0.086	6.2
N159W	H_2CO	$3_{03}-2_{02}$	0.788 (0.019)	236.78 (0.07)	5.82 (0.17)	0.127	6.2
	H_2CO	$3_{22}-2_{21}$	0.101 (0.017)	237.00 (0.30)	3.65 (0.70)	0.026	6.4
	H_2CO	$3_{21}-2_{20}$	0.105 (0.017)	236.98 (0.53)	5.94 (1.00)	0.017	5.2
N159E	H_2CO	$3_{03}-2_{02}$	0.555 (0.017)	234.53 (0.09)	5.84 (0.21)	0.090	4.9
	H_2CO	$3_{22}-2_{21}$	0.112 (0.018)	234.45 (0.47)	6.46 (1.37)	0.016	4.3
	H_2CO	$3_{21}-2_{20}$	0.073 (0.016)	232.94 (0.59)	5.36 (1.53)	0.013	3.9
	$C^{18}O$	2 – 1	0.231 (0.019)	234.85 (0.23)	6.17 (0.66)	0.035	4.8
N159S	H_2CO	$3_{03}-2_{02}$	0.056 (0.010)	235.87 (0.45)	4.45 (0.80)	0.012	3.9
	H_2CO	$3_{22}-2_{21}$	<0.005	...	...	...	4.9
	H_2CO	$3_{21}-2_{20}$	<0.005	...	...	...	3.4
	$C^{18}O$	2 – 1	0.161 (0.006)	236.35 (0.07)	3.27 (0.19)	0.047	3.4
			0.047 (0.006)	232.39 (0.30)	3.40 (0.52)	0.013	3.4

Notes.
(a) Values in parenthesis are standard deviations from Gaussian fits using CLASS as part of the GILDAS software.
(b) Full width to half maximum line width.

3. Results

The three para-H_2CO lines are detected in all sources except N159S. There, only the strongest para-H_2CO line, the 3_{03}-2_{02} transition, is detected. $C^{18}O$ (2-1), measured in 30 Dor, N159E, N159S, and N44BC, is detected in all sources. The para-H_2CO and $C^{18}O$ line spectra are presented in Figure 1. Line parameters are listed in Table 2, where velocity-integrated intensity, $\int T_{mb} dv$, local standard of rest velocity, V_{lsr}, full width to half maximum line width, FWHM, peak main beam brightness temperature, T_{mb}, and rms noise, were obtained from Gaussian fits.

3.1. Kinetic temperature and spatial density

To determine gas kinetic temperatures and spatial densities, we use the RADEX non-LTE model (van der Tak et al. 2007) offline code[2] with H_2CO collision rates from Wiesenfeld & Faure (2013) and $C^{18}O$ collision rates from Yang et al. (2010). The RADEX code needs five input parameters: background temperature, kinetic temperature, H_2 density, column density, and line width. For the background temperature, we adopt 2.73 K. Model grids for the para-H_2CO and $C^{18}O$ lines encompass 30 densities ($n(H_2) = 10^3 - 10^7$ cm^{-3}) and 30 temperatures ranging from 10 to 110 K. For the line width, we use the observed line width value (Table 2). The total beam averaged column density of $C^{18}O$ can be obtained from the $J = 2$–1 integrated intensity following Batrla & Wilson (2003).

$$N(C^{18}O) = 5.3 \times 10^{14} \int T_{mb}(C^{18}O, J = 2-1) dv, \quad (1)$$

where $\int T_{mb}(C^{18}O, J = 2-1) dv$ is the $C^{18}O$ (2-1) integrated intensity. The results are listed in Table 3. In the LMC, the gas is well mixed so that isotope ratios are pretty much the same throughout the galaxy (Johansson et al. 1994; Chin et al. 1997; Heikkilä et al. 1998, 1999; Wang et al. 2009). In the local ISM, the $^{16}O/^{18}O$ ratio is approximately 500 (Wilson & Rood 1994). We have, however, to keep in mind that fractional abundances in the LMC differ from those in the local ISM. In the LMC, ^{18}O is underabundant with respect to ^{16}O by about a factor of ~4 ($^{16}O/^{18}O$ ~2000 in the LMC, Chin 1999; Wang et al. 2009), while ^{18}O is underabundant by a factor of ~2.4 with respect to ^{17}O (locally, $^{18}O/^{17}O$ ~4.1, Zhang et al. 2007; Wouterloot et al. 2008; in the LMC ~1.7, Heikkilä et al. 1998; Wang et al. 2009). Therefore, $N(H_2)/N(C^{18}O)$ ratios should be higher by a factor of ~3 in the LMC with respect to the local ISM. This correlation will be used to derive H_2 column densities. The results for the H_2 column density are listed in Table 3. Assuming a CO to H_2 conversion factor of $X_{CO} \sim 4 \times 10^{20}$ cm^{-2} (K km s^{-1})$^{-1}$ for the LMC (Pineda et al. 2009; Wang et al. 2009), we can also derive a column density of $N(H_2)$ from the CO(1-0) integrated intensity moment map reported by Wong et al. (2011). The results of $N(H_2)$ are listed in Table 3. The H_2 column densities derived from $C^{18}O$ and CO are consistent with in the estimated uncertainty by a factor of two.

Previous observational results on transitions of $C^{18}O$ (1-0, 2-1) and para-H_2CO (2_{02}-1_{01}, 3_{03}-2_{02}, 3_{22}-2_{21} and 3_{21}-2_{20}) using the 15 m Swedish-ESO Submillimetre Telescope (SEST) show that the column density ratio of $N(C^{18}O)/N$(para-H_2CO) is ~ 100 in dense clumps of the LMC (Heikkilä et al. 1998, 1999; Wang et al. 2009). Assuming that the $N(C^{18}O)/N$(para-H_2CO) ratio is the same in our sample, we estimate the column density

[2] http://var.sron.nl/radex/radex.php

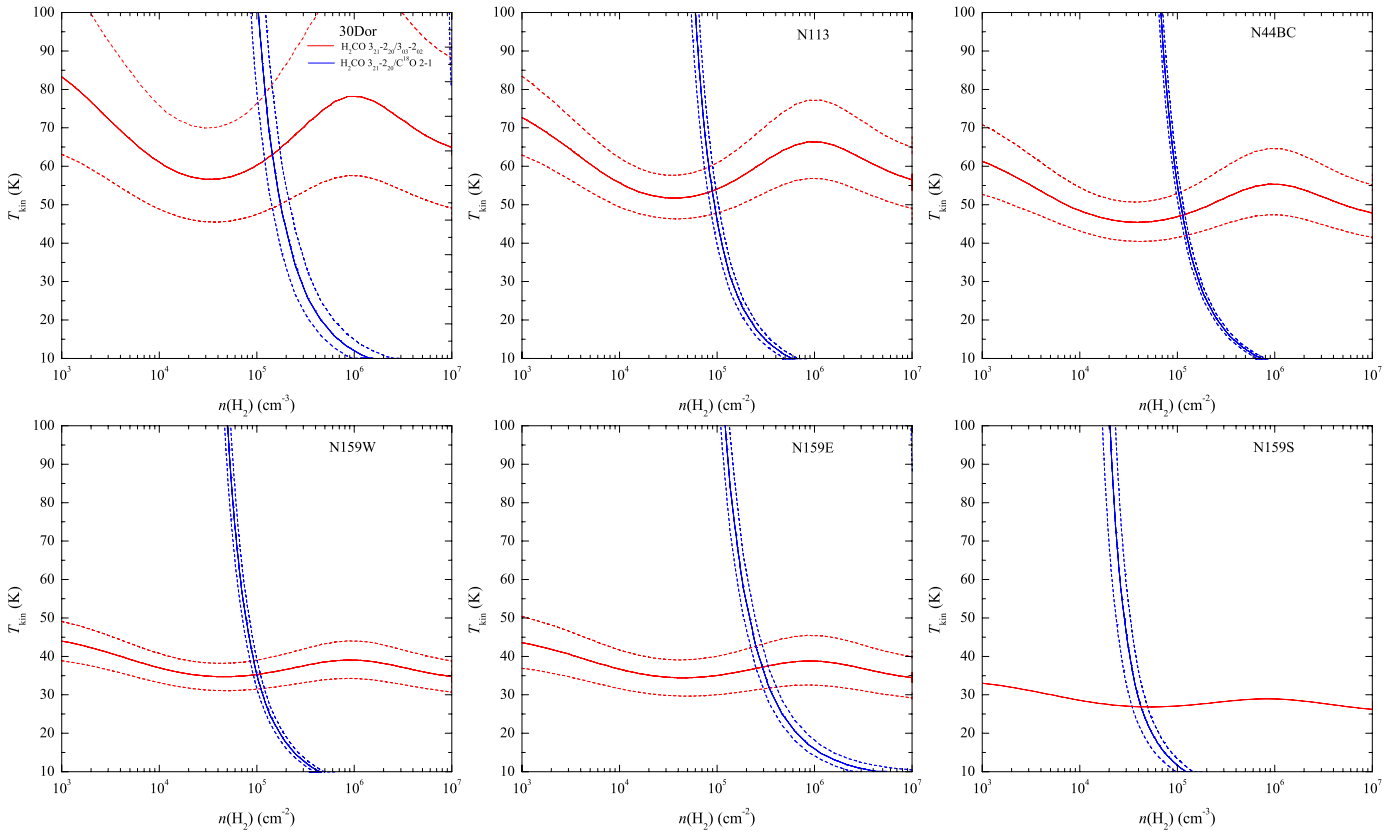

Fig. 2. RADEX non-LTE modeling of the gas kinetic temperature and spatial density, using the para-H_2CO 3_{21}-2_{20}/3_{03}-2_{02} (red solid and dashed lines are observed values and uncertainties) and para-H_2CO 3_{03}-2_{02}/$C^{18}O$ 2-1 (blue solid and dashed lines) integrated intensity ratios. For details, see the notes to Table 3.

of para-H_2CO from the $N(C^{18}O)$ column density. The results are listed in Table 3.

The para-H_2CO (3_{03}-2_{02}) line is the strongest of the three 218 GHz para-H_2CO transitions observed by us. In order to avoid small uncertain values in the denominator, the para-H_2CO 3_{22}-2_{21}/3_{03}-2_{02} and 3_{21}-2_{20}/3_{03}-2_{02} ratios are most suitable to derive the kinetic temperature. The para-H_2CO 3_{22}-2_{21} and 3_{21}-2_{20} transitions have similar energy above the ground state, $E_u \simeq 68$ K, similar line brightness, and are often detected at the same time (e.g., Mühle et al. 2007; Bergman et al. 2011; Wang et al. 2012; Lindberg & Jørgensen 2012; Ao et al. 2013; Immer et al. 2014, 2016; Treviño-Morales et al. 2014; Ginsburg et al. 2016; Tang et al. 2016); therefore, para-H_2CO 3_{22}-2_{21}/3_{03}-2_{02} and 3_{21}-2_{20}/3_{03}-2_{02} ratios are both good thermometers to determine the gas temperature. The kinetic temperature is traced by these two ratios with an uncertainty of $\lesssim$ 25% below 50 K (Mangum & Wootten 1993). While at $n(H_2)$ $\gtrsim 10^5$ cm^{-3} both ratios are similarly suitable, the para-H_2CO 3_{22}-2_{21}/3_{03}-2_{02} line ratio is affected by gas density at $n(H_2)$ $< 10^5$ cm^{-3} (Tang et al. 2016). For our sample, spatial density measurements probed by molecular tracers like CS, SO, CO, CI, H_2CO, HCO^+, and HCN (Heikkilä et al. 1998, 1999; Kim et al. 2004; Wang et al. 2009) show a range of 0.3 – 10 $\times$ 10^5 cm^{-3}. Therefore, in this work we use the para-H_2CO 3_{21}-2_{20}/3_{03}-2_{02} integrated intensity ratio to derive the kinetic temperature (Ginsburg et al. 2016; Immer et al. 2016).

In our Galaxy, spatial densities, $n(H_2)$, derived from para-H_2CO (3_{03}-2_{02}) are higher than from $C^{18}O$ (2-1). However, in the LMC, with lower density regions often being photoionized, this may be different. Therefore, here the para-H_2CO 3_{03}-2_{02}/$C^{18}O$ 2-1 integrated intensity ratio is used to constrain the spatial density assuming the two tracers have a similar spatial extent and sample the same region. For both lines we find similar line parameters (e.g., V_{lsr}, FWHM, see Table 2) in our sample, so our assumption is reasonable. igure 2 shows how the parameters are constrained by the line ratio distribution of para-H_2CO 3_{21}-2_{20}/3_{03}-2_{02} and para-H_2CO 3_{03}-2_{02}/$C^{18}O$ 2-1 in the T_{kin}-$n(H_2)$ parameter space. The determined results are listed in Table 3. The spatial density of our sample derived from the para-H_2CO 3_{03}-2_{02}/$C^{18}O$ 2-1 ratio shows a relatively narrow range of 0.4 – 2.9 $\times$ 10^5 cm^{-3} with an average of 1.5 $\pm$ 0.4 $\times$ 10^5 cm^{-3} (see Figure 2 and Table 3; errors given here and elsewhere are unweighted standard deviations of the mean), which is consistent with the results for the same dense clumps found from observations of e.g., SO, HCO^+, c-C_3H_2, CH_3OH, and H_2CO (Heikkilä et al. 1999; Wang et al. 2009).

As already mentioned, our three para-H_2CO (3-2) transitions are sensitive to gas at density $\sim 10^5$ cm^{-3} (Immer et al. 2016). To highlight how much the derived kinetic temperature depends on the derived density based on the admittedly uncertain assumption that para-H_2CO 3_{03}-2_{02} and $C^{18}O$ 2-1 trace the same gas, we have plotted in Figure 3 the relation between kinetic temperature and the para-H_2CO 3_{21}-2_{20}/3_{03}-2_{02} ratio at spatial density $n(H_2) = 10^5$ cm^{-3} with column density of N(para-H_2CO) = 2.1 $\times$ 10^{12} cm^{-2} and line width of 6 km s^{-1} (these are rough average values for our sample) using RADEX. Comparing this with the actually obtained values for individual sources derived from our para-H_2CO 3_{21}-2_{20}/3_{03}-2_{02} and para-H_2CO 3_{03}-2_{02}/$C^{18}O$ 2-1 ratios, the plot demonstrates that the temperatures derived in the two different ways are in a good agreement.

Table 3. Integrated intensity ratios, column densities, spatial densities, and temperatures.

Sources	3_{21}-2_{20} / 3_{03}-2_{02}	H_2CO 3_{03}-2_{02} / $C^{18}O$ 2-1	$N(C^{18}O)$ $\times10^{14}$ cm^{-2}	N(para-H_2CO) $\times10^{12}$ cm^{-2}	$N(H_2)$ $C^{18}O$ $\times10^{22}$ cm^{-2}	$N(H_2)$ CO $\times10^{22}$ cm^{-2}	$n(H_2)$ $\times10^5$ cm^{-3}	T_{kin} K	T_{LTE} K	T_{dust}[c] K
30 Dor	0.27±0.05	2.12±0.32	1.0	1.0	0.7	0.6	$1.45^{+0.69}_{-0.42}$	$63.0^{+18.2}_{-13.9}$	70.4	70–75
N113[a]	0.23±0.03	1.22±0.12	2.7	2.7	2.0	1.0	$0.89^{+0.18}_{-0.15}$	$53.6^{+6.7}_{-6.1}$	54.1	30–51
N44BC	0.20±0.03	1.39±0.07	3.0	3.0	2.1	1.3	$1.13^{+0.18}_{-0.16}$	$47.3^{+6.0}_{-5.4}$	45.9	35–45
N159W[b]	0.13±0.02	1.01±0.08	3.7	3.7	2.7	1.8	$1.00^{+0.20}_{-0.14}$	$35.3^{+3.7}_{-3.8}$	32.0	30–40
N159E	0.13±0.03	2.39±0.21	1.2	1.2	0.9	0.8	$2.92^{+1.15}_{-0.71}$	$37.2^{+5.9}_{-5.7}$	46.4	30–40
N159S	<0.085	0.35±0.07	0.9	0.9	0.6	1.4	>0.43	<26.9	<25.1	20–30

Notes.
Column 4: Obtained from equation (1).
Column 5: Para-H_2CO column densities adopting $N(C^{18}O)/N(\text{para-}H_2CO) = 100$ (see Section 3.1).
Column 6: H_2 column density derived from $C^{18}O$ with $X(C^{18}O/H_2) = 4.2 \times 10^{-8}$ (Frerking et al. 1982) and using the factor 3 correction explained in Section 3.1.
Column 7: H_2 column density obtained from ^{12}CO(1-0) with a conversion factor of $X_{CO} = 4 \times 10^{20}$ cm^{-2} (K km s^{-1})$^{-1}$ (see Section 3.1).
Column 9: T_{kin} derived with the density given in column (8).
[a]N113: Para-H_2CO 3_{03}-2_{02}/$C^{18}O$ 2-1 ratio data taken from Heikkilä et al. (1998) and Wang et al. (2009). $N(C^{18}O)$ derived from $C^{18}O$ 2-1 taken from Heikkilä et al. (1998).
[b]N159W: Para-H_2CO 3_{03}-2_{02}/$C^{18}O$ 2-1 ratio data taken from Heikkilä et al. (1998, 1999). $N(C^{18}O)$ derived from $C^{18}O$ 2-1 taken from Heikkilä et al. (1998). $N(H_2)$ data taken from Ott et al. (2010).
[c]Dust temperature references:
30 Dor: Werner et al. (1978); Heikkilä et al. (1999); Gordon et al. (2014);
N113: Wang et al. (2009); Gordon et al. (2014); Seale et al. (2014);
N44BC: Gordon et al. (2014);
N159W: Heikkilä et al. (1999); Bolatto et al. (2000); Gordon et al. (2014);
N159E: Gordon et al. (2014);
N159S: Gordon et al. (2014).
The upper and lower limits in columns 2, 8, 9, and 10 correspond to 3σ values.

Local thermodynamic equilibrium (LTE) is a good approximation for the H_2CO level populations under optically thin high-density conditions (Mangum & Wootten 1993; Watanabe & Mitchell 2008). Although LTE and RADEX non-LTE models use different approximations and assumptions, it is useful to check how the temperatures derived by the two methods compare. The para-H_2CO line intensity ratios 3_{22}-2_{21}/3_{03}-2_{02} and 3_{21}-2_{20}/3_{03}-2_{02} can be used to measure the LTE kinetic temperature because (see Section 1) the K_a = 0 and 2 ladders of para-H_2CO are mainly connected by collisions. The LTE kinetic temperature can be calculated assuming that the lines are optically thin, and originate from a high-density region (Mangum & Wootten 1993).

$$T_{\rm kin} = \frac{47.1}{ln(0.556\frac{I(3_{03}-2_{02})}{I(3_{22}-2_{21})})}, \quad (2)$$

where $I(3_{03}$-$2_{02})/I(3_{22}$-$2_{21})$ is the para-H_2CO integrated intensity ratio. The LTE kinetic temperatures are listed in Table 3. The uncertainty is $\lesssim$ 30% for this method of temperature measurement (Mangum & Wootten 1993). Considering this uncertainty, the temperatures derived from LTE and the RADEX non-LTE model are consistent with each other.

3.2. Individual sources

Below, results from the six sources covered by this study are individually discussed.

3.2.1. 30 Dor

Our three para-H_2CO and $C^{18}O$ 2-1 transitions have already been observed toward 30 Dor by Heikkilä et al. (1999) with the SEST (beam size ∼23″), but only para-H_2CO 3_{03}-2_{02} was detected. With our higher sensitivity we detect all four lines and confirm their para-H_2CO results. The kinetic temperature derived from para-H_2CO (3_{21}-2_{20}/3_{03}-2_{02}) is ∼63 K, which is the highest value determined in our sample. 30 Dor, hosting a cluster of O3 stars that rivals super star clusters, is the most spectacular star forming region in the Local Group (Walborn & Blades 1997; Massey & Hunter 1998), which makes such a high $T_{\rm kin}$ value comprehensible. The spatial density derived from the para-H_2CO 3_{03}-2_{02}/$C^{18}O$ 2-1 ratio is $\sim1.5 \times 10^5$ cm^{-3} at this temperature, which agrees with results derived from other species (e.g., CS, SO, HCO^+, Heikkilä et al. 1999).

3.2.2. N113

All three 218 GHz para-H_2CO lines as well as $C^{18}O$ 2-1 transition have been observed by Wang et al. (2009) and Heikkilä et al. (1998) with the SEST. Para-H_2CO 3_{03}-2_{02} and $C^{18}O$ 2-1 were detected. We detect the three transitions of para-H_2CO for the first time. The kinetic temperature derived from para-H_2CO (3_{21}-2_{20}/3_{03}-2_{02}) is ∼54 K. N113 is the LMC star forming region with the most luminous 22 GHz H_2O maser (Whiteoak & Gardner 1986; Lazendic et al. 2002; Oliveira et al. 2006), not quite as spectacular as 30 Dor, but hosts a few bright HII regions whose stellar energy feedback is likely to have elevated its temperature, thus leading to the second highest $T_{\rm kin}$ value. The spatial density derived from para-H_2CO 3_{03}-2_{02}/$C^{18}O$ 2-1 (ratio data from Wang et al. (2009) and Heikkilä et al. (1998), assuming that the para-H_2CO 3_{03}-2_{02}/$C^{18}O$ 2-1 ratio at the SEST beam size, ∼23″, is similar to that in the APEX beam size, ∼30″, see Section 3.2.4) is $\sim8.9 \times 10^4$ cm^{-3} at temperature ∼54 K, which agrees with results from other molecules (e.g., CS, HCO^+, HCN, Wang et al. 2009).

3.2.3. N44BC

$C^{18}O$ 2-1 has been detected in N44BC by Heikkilä et al. (1998) with the SEST. We detect the three 218 GHz para-H_2CO transitions and the $C^{18}O$ line. Our observations confirm their $C^{18}O$ 2-1 result. The kinetic temperature derived by para-H_2CO (3_{21}-2_{20}/3_{03}-2_{02}) is ~47 K. Such a high temperature likely results from the stellar energy feedback from the adjacent super bubble on the molecular cloud, which also shows bright mid-IR emission (Chen et al. 2009). The spatial density derived from the para-H_2CO 3_{03}-2_{02}/$C^{18}O$ 2-1 ratio is ~1.1×10^5 cm^{-3} at this temperature, which agrees with results from other molecules (e.g., CO, CI, Heikkilä et al. 1998; Kim et al. 2004).

3.2.4. N159W

The three para-H_2CO 218 GHz transitions as well as $C^{18}O$ 2-1 have been detected in N159W by Heikkilä et al. (1998, 1999) with the SEST. Our observations confirm their para-H_2CO results. The kinetic temperature derived by para-H_2CO (3_{21}-2_{20}/3_{03}-2_{02}) is ~35 K. The spatial density derived from the para-H_2CO 3_{03}-2_{02}/$C^{18}O$ 2-1 ratio (data from Heikkilä et al. 1998, 1999) is ~1.0×10^5 cm^{-3} at this temperature, which agrees with results measured by other species (e.g., CS, SO, Heikkilä et al. 1999). To quantify potential differences in temperature and density derived from APEX and SEST data, we determined the temperature and the density with the same method using the SEST para-H_2CO and $C^{18}O$ data from Heikkilä et al. (1998, 1999). The derived temperature and density are $30.3^{+5.7}_{-5.4}$ K and $1.14^{+0.35}_{-0.23} \times 10^5$ cm^{-3}, respectively. This indicates nearly the same spatial density and a few Kelvin difference for the kinetic temperature. This temperature difference is similar to its 1σ uncertainty (~6 K). Therefore, the temperature gradient and density gradient is small when moving from a beam size of 7.3 pc (APEX) to 5.6 pc (SEST).

3.2.5. N159E

The three para-H_2CO 218 GHz transitions as well as $C^{18}O$ 2-1 are detected. To our knowledge, it is the first detection of para-H_2CO in the N159E region. The source shows similar properties as N159W. The kinetic temperature derived from para-H_2CO (3_{21}-2_{20}/3_{03}-2_{02}) is ~37 K. The spatial density derived from the para-H_2CO 3_{03}-2_{02}/$C^{18}O$ 2-1 ratio is ~2.9×10^5 cm^{-3} at this temperature.

3.2.6. N159S

Two velocity components are detected by $C^{18}O$, at 232.4 and 236.4 km s^{-1}. Para-H_2CO 3_{03}-2_{02} is detected at a velocity of 235.9 km s^{-1} (see Table 2). However, the para-H_2CO 3_{22}-2_{21} and 3_{21}-2_{20} lines are not detected. The dust temperature ranges from 20 to 30 K (Gordon et al. 2014). N159S appears to be a cold cloud (Heikkilä et al. 1999), and has been shown to host no massive star formation at present and during the last 10 Myr (Chen et al. 2010). The upper limit to the kinetic temperature derived from para-H_2CO (3_{21}-2_{20}/3_{03}-2_{02}) based on our observational 3σ limit for the 3_{21}-2_{20} line is ~27 K. The spatial density derived from the para-H_2CO 3_{03}-2_{02}/$C^{18}O$ 2-1 ratio is >4.3 $\times 10^4$ cm^{-3}, which is consistent with results measured by other species (e.g., CS, SO, Heikkilä et al. 1999).

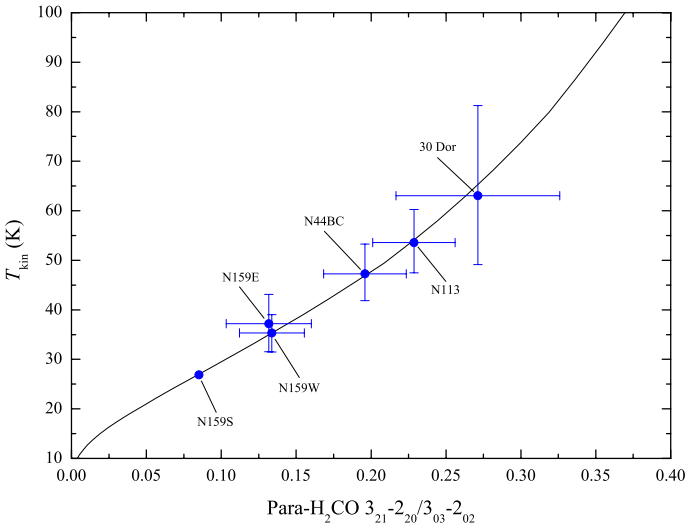

Fig. 3. RADEX non-LTE modeling of the relation between the gas kinetic temperature and the para-H_2CO 3_{21}-2_{20}/3_{03}-2_{02} integrated intensity ratio (solid line), assuming $n(H_2) = 10^5$ cm^{-3}, N(para-H_2CO) = 2.1 $\times 10^{12}$ cm^{-2}, and a line width of 6 km s^{-1}. Blue points are the results derived from the measured para-H_2CO 3_{21}-2_{20}/3_{03}-2_{02} and para-H_2CO 3_{03}-2_{02}/$C^{18}O$ 2-1 ratios. For N159S, 3σ upper limits for the line ratio and the kinetic temperature have been taken.

4. Discussion

4.1. Comparison of temperatures derived from H_2CO, CO, NH_3, and the dust

The kinetic temperatures of molecular clumps in the LMC have been calculated by multi-transition data of CO (Johansson et al. 1998; Heikkilä et al. 1999; Israel et al. 2003; Kim et al. 2004; Bolatto et al. 2005; Pineda et al. 2008; Mizuno et al. 2010; Minamidani et al. 2008, 2011; Fujii et al. 2014; Paron et al. 2016). These observations show that the higher temperatures ($T_{kin} \gtrsim 100$ K) occur in cloud regions that are of lower density ($\lesssim 10^3$ cm^{-3}) and that the gas is colder (T_{kin} = 10 – 80 K) in regions of higher density (10^4 – 10^5 cm^{-3}). As already mentioned in Section 3.1, the spatial density range of our sample derived from the para-H_2CO 3_{03}-2_{02}/$C^{18}O$ 2-1 ratio with respect to the Galaxy is 0.4 – 2.9 $\times 10^5$ cm^{-3} with an average of 1.5 ± 0.4 $\times 10^5$ cm^{-3}. Excluding the quiescent cloud N159S, where only one para-H_2CO line could be detected, the gas kinetic temperatures derived from para-H_2CO (3_{21}-2_{20}/3_{03}-2_{02}), range from 35 to 63 K with an average of 47 ± 5 K. Temperatures and densities derived from CO are for 30 Dor T_{kin} ~ 40 – 80 K and $n(H_2)$ ~ 3×10^3 – 3×10^5 cm^{-3} (Johansson et al. 1998; Heikkilä et al. 1999; Minamidani et al. 2008), N159W T_{kin} ~ 16 – >30 K and $n(H_2)$ ~ 3×10^3 – 8×10^5 cm^{-3} (Johansson et al. 1998; Heikkilä et al. 1999; Bolatto et al. 2005; Minamidani et al. 2008), N159E T_{kin} > 40 K and $n(H_2)$ ~ 1×10^3 – 3×10^5 cm^{-3} (Minamidani et al. 2008), and N159S T_{kin} ~ 10 – 60 K and $n(H_2)$ ~ 1×10^3 – 1×10^5 cm^{-3} (Heikkilä et al. 1999; Minamidani et al. 2008). Temperatures derived from para-H_2CO are consistent with but much more precise than the results derived from CO in the dense regions (>10^3 cm^{-3}).

Except for N159E, all our sources have been surveyed in NH_3 (1,1) and (2,2) by Ott et al. (2010). These lines are only detected in the massive star-forming region N159W. We compare fractional abundances of N(para-NH_3)/$N(H_2)$ and N(para-H_2CO)/$N(H_2)$ to column density $N(H_2)$ obtained from ^{12}CO(1-

0) in Figure 4. These show that formaldehyde has a stable fractional abundance ranging from 0.6 to 5.7 × 10^{-10} cm^{-2} with an average of 2.7 ± 1.8 × 10^{-10} cm^{-2} in molecular clouds of the LMC with $N(H_2)$ column densities ranging from 0.4 to 2 × 10^{22} cm^{-2}. Ammonia only survives in a high column density environment with $N(H_2) \sim 2 \times 10^{22}$ cm^{-2}. The fractional abundance of ammonia is $\sim 10^{-10} - 10^{-9}$ in N159W and M82, which is similar to that of formaldehyde in the LMC. As already mentioned, the kinetic temperature derived from the NH_3 (2,2)/(1,1) line ratio in N159W is ~16 K (Ott et al. 2010), which is two times lower than that derived from para-H_2CO. Previous para-H_2CO (3_{22}-2_{21}/3_{03}-2_{02}) and NH_3 (2,2)/(1,1) observations toward the starburst galaxy M82 also show significantly different gas kinetic temperatures (Weiß et al. 2001; Mühle et al. 2007). M82, a satellite galaxy like the LMC, shows a similar environment, involving low metallicity combined with a high UV flux. This only leaves NH_3 surviving in the most shielded pockets of molecular gas, resulting in a low fractional abundance (see Figure 4) and a low kinetic temperature. Furthermore, this abundance is demonstrating in an exemplary way that H_2CO is less affected by photodissociation, sampling a more extended region. Therefore, para-H_2CO traces in these instances a higher temperature than NH_3 (2,2)/(1,1). We conclude that para-H_2CO line ratios are a superior thermometer to trace dense gas temperatures in low metallicity galaxies with strong UV radiation. Nevertheless, more detailed spatially resolved comparisons of H_2CO with NH_3 temperatures would be very interesting because it could provide more information on temperature gradients and the location of different kinetic temperature layers.

The temperatures derived from dust and gas are often in agreement in the active and dense clumps of Galactic disk clouds (Dunham et al. 2010; Giannetti et al. 2013; Battersby et al. 2014). However, observed gas and dust temperatures do not agree with each other in the Galactic Central Molecular Zone (CMZ) and external galaxies (Güsten et al. 1981; Ao et al. 2013; Mangum et al. 2013a; Ott et al. 2014; Ginsburg et al. 2016; Immer et al. 2016). Dust temperatures in the LMC have been obtained by Gordon et al. (2014) using Herschel 100 to 500 μm dust continuum emission data. They range approximately from 13 to 73 K. For our sample, the dust temperatures range from 30 to 75 K (Werner et al. 1978; Heikkilä et al. 1999; Bolatto et al. 2000; Wang et al. 2009; Seale et al. 2014; Gordon et al. 2014) while the para-H_2CO derived temperature ranges from 35 to 63 K. The temperatures derived from para-H_2CO ratios and dust emission are therefore in good agreement (see Table 3). This indicates that the dust and H_2CO kinetic temperatures are equivalent in the star forming regions of the LMC. Assuming that H_2CO traces the bulk of the dense molecular gas and that ammonia shows very low abundances, this can be generalized in the sense that dense gas and dust temperatures are generally equivalent.

4.2. Star-forming regions in the Galaxy, the LMC, and other galaxies

The gas temperatures of ATLASGAL (APEX Telescope Large Area Survey of the GALaxy) massive star forming clumps have been measured by para-H_2CO (3_{03}-2_{02}, 3_{22}-2_{21}, and 3_{21}-2_{20}) line ratios (Tang et al. 2016). The thus derived gas kinetic temperatures at density n(H_2) = 10^5 cm^{-3} with size of 0.3 – 0.7 pc range from 30 to 61 K with an average of 46 ± 9 K, which agrees remarkably well with the results in the LMC with a beam size of ~7 pc. Large area mapping measurements of kinetic temperatures in the Galactic CMZ with the same transitions of para-

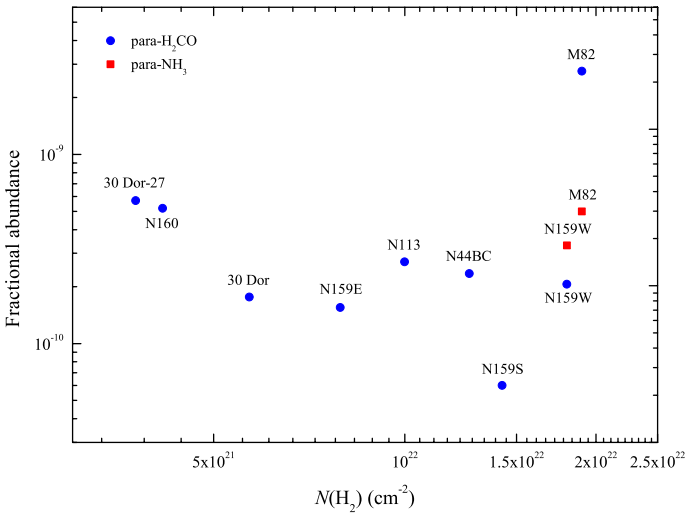

Fig. 4. Abundances of N(para-NH_3)/$N(H_2)$, red squares, and N(para-H_2CO)/$N(H_2)$, blue points, vs. column density $N(H_2)$ obtained from ^{12}CO. 30 Dor-27 and N160 data taken from Heikkilä et al. (1999). N159W data taken from Ott et al. (2010). M82 data taken from Weiß et al. (2001) and Mühle et al. (2007).

H_2CO (Ao et al. 2013; Ginsburg et al. 2016) suggest that the mean gas temperature is ~48 K at $n(H_2)$ = 10^5 cm^{-3} or ~65 K at $n(H_2)$ = 10^4 cm^{-3} in the whole ~300 pc surveyed region. It shows a higher T_{kin} value than our observed results. The spatial densities derived from the para-H_2CO 3_{03}-2_{02}/$C^{18}O$ 2-1 ratio in our sample agree with the observed results in the Galactic clumps (Beuther et al. 2002; Motte et al. 2003; Wienen et al. 2012, 2015), HII regions (Henkel et al. 1983; Ginsburg et al. 2011), and giant molecular clouds (GMCs) (Wadiak et al. 1988; Ginsburg et al. 2015; Immer et al. 2016). This agreement indicates that the physical conditions of the star forming regions should be similar in both the LMC and our Galactic disk.

Using the three transitions of para-H_2CO at ~218 GHz to measure the kinetic temperature of the starburst galaxy M82 shows that the derived kinetic temperature ($T_{kin}(H_2CO)$ ~ 200 K; Mühle et al. 2007) is significantly higher than in the LMC. Kinetic temperatures of starburst galaxies measured with multi-inversion transitions of NH_3 show a range from 24 to $\gtrsim$ 250 K (Henkel et al. 2000, 2008; Mauersberger et al. 2003; Ao et al. 2011; Lebrón et al. 2011; Mangum et al. 2013a). The temperatures derived from para-H_2CO line ratios in the LMC overlap with the values found for a sample at lower temperature (e.g., M83, NGC6946). This is likely due to the inclusion of higher excited ammonia lines, which, however, should be difficult to detect in the LMC because there particularly warm regions irradiated by enhanced UV radiation should be almost devoid of NH_3. The spatial densities in starburst galaxies derived from ortho-H_2CO (2_{11}-2_{12}/1_{10}-1_{11}) line ratios (Mangum et al. 2008, 2013b) show a similar range ($10^{4.5}$–$10^{5.5}$ cm^{-3}) to that derived from para-H_2CO 3_{03}-2_{02}/$C^{18}O$ 2-1 ratios in the LMC. This indicates that star formation in the LMC and external galaxies may arise from dense molecular gas (>10^4 cm^{-3}), but gas heating rates may be quite different.

4.3. Correlation of gas temperature with star formation

In star forming galaxies, a lack of correlation between the gas kinetic temperatures traced by NH_3 and star formation rate in-

dicated by infrared luminosity was found by Mangum et al. (2013a). To investigate how the kinetic temperatures traced by para-H_2CO correlate with star formation in the LMC, we compared the gas kinetic temperature to the Herschel 250 μm dust emission which indicates the infrared luminosity (Seale et al. 2014). We averaged the Herschel 250 μm data over a 30″ beam corresponding to our para-H_2CO data. A comparison between gas kinetic temperatures derived from para-H_2CO and the Herschel 250 μm flux is shown in Figure 5. It reveals a correlation of gas temperature and 250 μm flux for the five sources with all 218 GHz para-H_2CO lines detected (slope = 0.97 ± 0.49, correlation coefficient $R \sim 0.75$). According to the relation between the infrared luminosity and 250 μm flux $L_{\rm FIR} \propto F_{\rm S250}^{1.2}$ in the LMC (Seale et al. 2014), the infrared luminosity and the gas temperature derived from para-H_2CO are related by a power-law of the form $L_{\rm FIR} \propto T_{\rm kin}^{1.2\pm0.59}$ where the power-law index is lower than that of the Stefan-Boltzmann law ($L \propto T_{\rm kin}^4$). This suggests that this picture is an oversimplification, and that star formation occurs in extended regions leading to the formation of stellar clusters with multiple FIR sources (e.g., Chen et al. 2009, 2010). Assuming that the 250 μm flux is mostly coming from clusters of FIR sources distributed across the regions from where the H_2CO emission is arising, this can be generalized in the sense that the gas heating mechanism must be related to the formation of young massive stars. To find out whether the bulk of the H_2CO emission is originating from within individual clusters of FIR sources, in between adjacent such FIR clusters, or both, higher resolution H_2CO observations would be mandatory.

We need more data points in the LMC to understand the relationship between $T_{\rm kin}$ and star formation and to then apply this relationship to more distant galaxies with ALMA. Para-H_2CO 3_{21}-2_{20}/3_{03}-2_{02} and para-H_2CO 3_{03}-2_{02}/$C^{18}O$ 2-1 line ratios provide a direct estimate of the gas kinetic temperatures and spatial densities for molecular gas on a scale of ∼7 pc in the star forming regions of the LMC. It would be meaningful to use these line ratios to measure the physical properties of the dense molecular gas at smaller linear scales with ALMA and to start systematic investigations in more distant star-forming galaxies.

5. Summary

We have measured the kinetic temperature and spatial density with para-H_2CO ($J_{K_AK_C}$ = 3_{03}-2_{02}, 3_{22}-2_{21}, and 3_{21}-2_{20}) line ratios and the $C^{18}O$ 2-1 line in massive star-forming regions of the LMC. Kinetic temperatures derived from the above mentioned formaldehyde 218 GHz line triplet are compared with those obtained from the dust and, in one case, also from ammonia using the 12-m APEX telescope. The main results are the following:

1. Using the RADEX non-LTE program, we derive gas kinetic temperatures and spatial densities modeling the measured para-H_2CO 3_{21}-2_{20}/3_{03}-2_{02} and para-H_2CO 3_{03}-2_{02}/$C^{18}O$ 2-1 line ratios.
2. The gas kinetic temperatures derived from para-H_2CO (3_{21}-2_{20}/3_{03}-2_{02}) line ratios of the star forming regions in the LMC are warm, ranging from 35 to 63 K with an average of 47 ± 5 K, which is similar to that obtained from Galactic disk massive star forming clumps.
3. The spatial density derived from the para-H_2CO 3_{03}-2_{02}/$C^{18}O$ 2-1 ratio shows a range of 0.4 – 2.9 × 10^5 cm^{-3} with an average of 1.5 ± 0.4 × 10^5 cm^{-3}. It agrees with results measured by ortho-H_2CO (2_{11}-2_{12}/1_{10}-1_{11}) line ratios in Galactic regions of massive star formation.

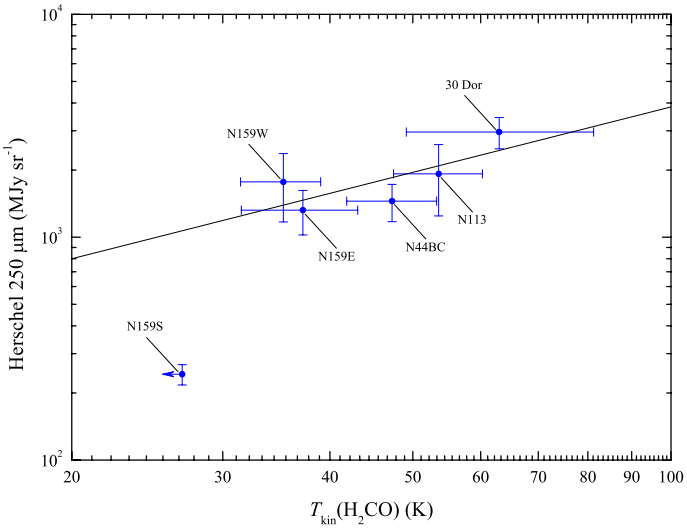

Fig. 5. Comparison of gas kinetic temperatures derived from para-H_2CO 3_{21}-2_{20}/3_{03}-2_{02} against the Herschel 250 μm flux. The straight line is the result from a linear fit for the five sources with all 218 GHz para-H_2CO lines detected. N159S provides with respect to $T_{\rm kin}$ a 3σ upper limit. Thus this point may actually be located much further to the left, closer to the linear fit obtained from the other five sources.

4. Temperatures derived from the para-H_2CO line ratios agree with those derived from CO in dense regions ($n(H_2) > 10^3$ cm^{-3}). The gas temperature derived from the NH_3 (2,2)/(1,1) line ratio is ∼16 K in N159W (Ott et al. 2010), which is two times lower than the temperature derived from the para-H_2CO line ratio and the dust. Ammonia only survives in the most shielded pockets of molecular gas in the LMC′s low metallicity environment affected by a high UV flux. Formaldehyde is less affected by photodissociation and traces a more extended region.
5. A comparison of the gas kinetic temperature derived from para-H_2CO and the temperature obtained from dust emission shows good agreement. It indicates that the bulk of the dense gas and dust are in approximate thermal equilibrium in the dense star formation regions of the LMC.
6. A correlation between the gas kinetic temperatures derived from para-H_2CO and infrared luminosity indicated by the 250 μm flux suggests that our kinetic temperatures traced by para-H_2CO are closely associated with extended star formation in the LMC.

Acknowledgements. We thank the staff of the APEX telescope for their assistance in observations. The authors are also thankful for the helpful comments of the anonymous referee. This work was funded by The National Natural Science Foundation of China under grant 11433008 and The Program of the Light in China′s Western Region (LCRW) under grant Nos.XBBS201424 and The National Natural Science Foundation of China under grant 11373062. C.H acknowledges support by a visiting professorship for senior international scientists of the Chinese Academy of Sciences (2013T2J0057). This research has used NASA's Astrophysical Data System (ADS).

References

Ao, Y., Henkel, C., Menten, K. M., et al. 2013, A&A, 550, 135
Ao, Y., Henkel, C., Braatz, J. A., et al. 2011, A&A, 529, 154
Baan, W. A., Güsten, R., & Haschick, A. D. 1986, ApJ, 305, 830
Baan, W. A., Haschick, A. D., & Uglesich, R. 1993, ApJ, 415, 140
Baan, W. A., Henkel, C., Schilke, P., et al. 1990, ApJ, 353, 132
Batrla, W. & Wilson, T. L. 2003, A&A, 408, 231

Battersby, C., Bally, J., Dunham, M., et al. 2014, ApJ, 786, 116
Benson, P. J., & Myers, P. C. 1983, ApJ, 270, 589
Bergman, P., Parise, B., Liseau, R., & Larsson, B. 2011, A&A, 527, 39
Beuther, H., Schilke, P., Menten, K. M., et al. 2002, ApJ, 566, 945
Bieging, J. H., Wilson, T. L., & Downes, D. 1982, A&AS, 49, 607
Bolatto, A. D., Israel, F. P., & Martin, C. L. 2005, ApJ, 633, 210
Bolatto, A. D., Jackson, J. M., Israel, F. P., et al. 2000, ApJ, 545, 234
Caselli, P., Hasegawa, T. I., & Herbst, E. 1993, ApJ, 408, 548
Chen, C.-H. R., Chu, Y. H., Gruendl, R. A. et al. 2009, ApJ, 695, 511
Chen, C.-H. R., Indebetouw, R., Chu, Y. H. et al. 2010, ApJ, 721, 1206
Chin, Y. 1999, IAUS, 190, 279
Chin, Y. N., Henkel, C., Whiteoak, J. B. et al. 1997, A&A, 317, 548
Chira, R. A., Beuther, H., Linz, H., et al. 2013, A&A, 552, 40
Cohen, R. J., & Few, R. W. 1981, MNRAS, 194, 711
Cohen, R. J., Matthews, N., Few, R. W., et al. 1983, MNRAS, 203, 1123
Danby, G., Flower, D. R., Valiron, P., et al. 1988, MNRAS, 235, 229
Downes, D., Wilson, T. L., Bieging, J., & Wink, J. 1980, A&AS, 40, 379
Dunham, M. K., Rosolowsky, E., Evans, N. J. II., et al. 2010, ApJ, 717, 1157
Fujii, K., Minamidani, T., Mizuno, N., Onishi, T., et al. 2014, ApJ, 796, 123
Frerking, M. A., Langer, W. D., & Wilson, R. W. 1982, ApJ, 262, 590
Giannetti, A., Brand, J., Sánchez-Monge, Á., et al. 2013, A&A, 556, 16
Ginsburg, A., Bally, J., Battersby, C., et al. 2015, A&A, 573, 106
Ginsburg, A., Darling, J., Battersby, C., et al. 2011, ApJ, 736, 149
Ginsburg, A., Henkel, C., Ao, Y., et al. 2016, A&A, 586, 50
Gordon, K. D., Roman-Duval, J., Bot, C., et al. 2014, ApJ, 797, 85
Guo, W. H., Esimbek, J., Tang, X. D., et al. 2016, Ap&SS, 361, 264
Güsten, R. & Henkel, C. 1983, A&A, 125, 136
Güsten, R., Walmsley, C. M., & Pauls, T. 1981, A&A, 103, 197
Heikkilä, A., Johansson, L. E. B., & Olofsson, H. 1998, A&A, 332, 493
Heikkilä, A., Johansson, L. E. B., & Olofsson, H. 1999, A&A, 344, 817
Henkel, C., Baan, W. A., & Mauersberger, R. 1991, A&ARv, 3, 47
Henkel, C., Braatz, J. A., Menten, K. M., & Ott, J. 2008, A&A, 485, 451
Henkel, C., Mauersberger, R., Peck, A. B., et al. 2000, A&A, 361L, 45
Henkel, C., Wilson, T. L., Walmsley, C. M., & Pauls, T. 1983, A&A, 127, 388
Hidaka, H., Watanabe, N., Shiraki,T., et al. 2004, ApJ, 614, 1124
Ho P. T. P., & Townes C . H., 1983, ARA&A, 21, 239
Hüttemeister, S., Mauersberger, R., & Henkel, C., 1997, A&A, 326, 59
Immer, K., Galván-Madrid, R., König, C., et al. 2014, A&A, 572, 63
Immer. K, Kauffmann. J., Pillai. T., et al. 2016, A&A, 595, 94
Israel, F. P., Johansson, L. E. B., Rubio, M., et al. 2003, A&A, 406, 817
Johansson, L. E. B., Greve, A., Booth, R. S., et al. 1998, A&A, 331, 857
Johansson, L. E. B., Olofsson, H., Hjalmarson, A., et al. 1994, A&A, 291, 89
Johnstone, D., Boonman A. M. S. & van Dishoeck E. F. 2003. A&A, 412, 157
Johnston, K. G., Beuther, H., Linz, H., et al. 2014, A&A, 568, 56
Kim, S., Walsh, W., & Xiao, K. 2004, ApJ, 616, 865
Lazendic, J. S., Whiteoak, J. B., Klamer, I., et al. 2002, MNRAS, 331, 969
Lebrón, M., Mangum, J. G., Mauersberger, R. et al. 2011, A&A, 534, 56
Lindberg, J. E., & Jørgensen, J. K. 2012, A&A, 548, 24
Mangum, J. G., Darling, J., Henkel, C., et al. 2013a, ApJ, 779, 33
Mangum, J. G., Darling, J., Henkel, C., & Menten, K. M. 2013b, ApJ, 766, 108
Mangum, J. G., Darling, J., Menten, K. M., & Henkel, C. 2008, ApJ, 673, 832
Mangum, J. G., & Wootten, A. 1993, ApJS, 89, 123
Mangum, J. G., Wootten, A., & Plambeck, R. L. 1993, ApJ, 409, 282
Mangum, J. G., Wootten, A., Wadiak, E. J., & Loren, R. B. 1990, ApJ, 348, 542
Massey, P., & Hunter, D. A. 1998, ApJ, 493, 180
Mauersberger, R., Henkel, C., Weiß, A., et al. 2003, A&A, 403, 561
Mauersberger, R., Henkel, C., & Wilson, T. L. 1987, A&A, 173, 352
Minamidani, T., Mizuno, N., Mizuno, Y., et al. 2008, ApJS, 175, 485
Minamidani, T., Tanaka, T., Mizuno, Y., et al. 2011, AJ, 141, 73
Mitchell, G. F., Johnstone, D., Moriarty-Schieven, G., et al. 2001, ApJ, 556, 215
Mizuno, Y., Kawamura, A., Onishi, T., et al. 2010, PASJ, 62, 51
Motte, F., Schilke, P., & Lis, D. C. 2003, ApJ, 582, 277
Mühle, S., Seaquist, E. R., & Henkel, C. 2007, ApJ, 671, 1579
Oliveira, J. M., van Loon, J. Th., Stanimirović, S., & Zijlstra, A. A. 2006, MNRAS, 372, 1509
Ott, J., Henkel, C., Braatz, J. A., & Weiß, A. 2011, ApJ, 742, 95
Ott, J., Henkel, C., Staveley-Smith, L., & Weiß, A. 2010, ApJ, 710, 105
Ott, J., Weiß, A., Staveley-Smith, L., et al. 2014, ApJ, 785, 16
Paron, S., Ortega, M. E., Fariña, C., et al. 2016, MNRAS, 455, 518
Pineda, J. L., Mizuno, N., Stutzki, J., et al. 2008, A&A, 482, 197
Pineda, J. L., Ott, J., Klein, U., et al. 2009, ApJ, 703, 736
Pietrzyński, G., Graczyk, D., Gieren, W., et al. 2013, Natur, 495, 76
Qin, S. L., Zhao, J. H., Moran, J. M., et al. 2008, ApJ, 677, 353
Rolleston, W. R. J., Trundle, C., & Dufton, P. L. 2002,A&A, 396, 53
Seale, J. P., Meixner, M., Sewiło, M., et al. 2014, AJ, 148, 124
van der Tak, F. F. S., Black, J. H., Schier, F. L., et al. 2007, A&A, 468, 627
Tang, X. D., Esimbek, J., Zhou, J. J., et al. 2013, A&A, 551, 28
Tang, X. D., Henkel, C., Menten, K. M., et al. 2016, arXiv, 1610, 05548
Treviño-Morales, S. P., Pilleri, P., Fuente, A., et al. 2014, A&A, 569, 19
Wadiak, E. J., Rood, R. T., & Wilson, T. L. 1988, ApJ, 324, 931
Walborn, N. R., & Blades, J. C. 1997, ApJS, 112, 457
Walmsley, C. M., & Ungerechts, H. 1983, A&A, 122, 164
Wang, M., Chin, Y.-N., Henkel, C., et al. 2009, ApJ, 690, 580
Wang, M., Henkel, C., Chin, Y.-N., et al. 2004, A&A, 422, 883
Wang, Y., Beuther, H., Zhang, Q., et al. 2012, ApJ, 754, 87
Watanabe, N., & Kouchi, A. 2002, ApJ, 571, 173
Watanabe, T., & Mitchell, G. 2008, AJ, 136, 1947
Weiß, A., Neininger, N., Henkel, C., Stutzki, J., & Klein, U. 2001, ApJ, 554, 143
Werner M.W., Becklin E.E., Gatley I., et al., 1978, MNRAS 184, 365
Westerlund B.E., 1990, A&AR 2, 29
Whiteoak, J. B. & Gardner, F. F. 1976, MNRAS, 174, 51
Whiteoak, J. B., & Gardner, F. F. 1986, MNRAS, 222, 513
Wiesenfeld, L., & Faure, A. 2013, MNRAS, 432, 2573
Wienen, M., Wyrowski, F., Menten, K. M., et al. 2015, A&A, 579, 91
Wienen, M., Wyrowski, F., Schuller, F., et al. 2012, A&A, 544, 146
Wilson, T. L. & Rood, R. 1994, ARA&A, 32, 191
Wong, T., Hughes, A., Ott, J., et al. 2011, ApJS, 197, 16
Woon, D. 2002, ApJ, 569, 541
Wouterloot, J. G. A., Henkel, C., Brand, J., Davis, G. R. 2008, A&A, 487, 237
Yang, B., Stancil, P.C., Balakrishnan, N., & Forrey, R. C. 2010, ApJ, 718, 1062
Zhang, J. S., Henkel, C., Mauersberger, R., et al. 2007, A&A, 465, 887
Zhang, C., P., Esimbek, J., Zhou, J. J., et al. 2012, Ap&SS, 337, 283
Zylka, R., Güsten, R., Henkel, C., & Batrla, W. 1992, A&AS, 96, 525